The Design Process for Wheel-Robot Integration

by

Michael Angelo Carvajal

Submitted to the Department of Mechanical Engineering
in partial fulfillment of the requirements for the degree of

Bachelor of Science in Mechanical Engineering

at the

MASSACHUSETTS INSTITUTE OF TECHNOLOGY

June 2009

Author .. ..
Department of Mechanical Engineering
May 12, 2009

Certified by .....
William J. Mitchell
Professor of Architecture and Media Arts and Sciences
Thesis Supervisor

Accepted by .....
John H. Lienhard V
Professor of Mechanical Engineering
Chairman, Undergraduate Thesis Committee

The Design Process for Wheel-Robot Integration

by

Michael Angelo Carvajal

Submitted to the Department of Mechanical Engineering
on May 12, 2009, in partial fulfillment of the
requirements for the degree of
Bachelor of Science in Mechanical Engineering

Abstract

In this thesis, the design process for wheel-robot integration was documented and reflected on. The project focused on redesigned certain aspects a half-scale wheel-robot to be integrated with a half-scale CityCar prototype being built by the MIT Media Lab's Smart Cities Group. Primary attention was spent on analyzing the required steering torque need to maneuver the half-scale vehicle, and on implementing a design where the wheel-robots steered about the axis that passed through the center of gravity of the tire component. Budget and time constraints required quick and easy solutions to the design and integration of the wheel-robot components. A half-scale prototype made by Media Lab graduate student Peter Schmitt was used as a benchmark for the new wheel-robot design and an analysis of Schmitt's prototype is documented. Though many ideas and concept variations were explored during the design process, a complete design of the wheel-robot was not finalized in time for this report. More time must be spent in order to finalized an integration process that can be scaled up to the full-scale CityCar for future use in urban mobility improvement.

Thesis Supervisor: William J. Mitchell
Title: Professor of Architecture and Media Arts and Sciences

Acknowledgments

I am very grateful to everyone who has guided me during my time here at MIT. In particular, I would like to thank the following individuals.

-My family, first and foremost. I would like to thank my loving mother for always telling me I could do anything I put my mind to. She gave up so much in her life to see that my siblings and I had a better one, and I couldn't ask for anything more. I would like to thank my older brother, Nelson, my sister, Samantha, and my little brother, Anthony, for supporting me in all of my efforts.

-Irmina, the love of my life. She bore the burden of letting me come to this school, a thousand miles away, and yet she has always been there for me. I could not ask for a better person to spend the rest of my life with, and I thank her for her undying spirit and unconditional love.

-My friends back home in Chicago for all the good times we had and will have in the future. I would like to thank my friends and peers here at MIT, in particular Tiffany Tseng and Brian Demers. I am grateful for their reliable friendship and for sharing my interest. I thank Greg Schroll for being the engineer I aspire to be and for always checking up on me even after graduating. I could not have survived these past four years without them.

-Professor Mitchell, Retro Poblano, and the SmartCities Group at the MIT Media Lab for allowing me to work with them on this project. My thanks to Jeff Disko for taking the time to proofread my thesis at such a late hour.

Finally, I would like to thank MIT and its Department of Mechanical Engineering staff and courses for exposing me to so a new world full of possibilities. I will never forget my time here and would love to experience more of this spectacular environment in the future.

THIS PAGE INTENTIONALLY LEFT BLANK

Contents

THIS PAGE INTENTIONALLY LEFT BLANK

List of Figures

THIS PAGE INTENTIONALLY LEFT BLANK

List of Tables

THIS PAGE INTENTIONALLY LEFT BLANK

Chapter 1

Introduction

The Smart Cities Group, a researching group at the MIT Media Lab, decided to build a functional, half-scale version of their CityCar concept over the course of the Spring 2009 semester. The primary focus of this project was to figure out how to improve on the design of the half-scale wheel-robot previously built by Peter Schmitt, a graduate student in the group. This thesis revolves the redesign of the half-scale vehicles wheel-robots by replacing their components and integrating them all to fit within the confined space provided by the vehicle. The original goal was to improve on the wheel-robot design, most notably by figuring out how to find a steering actuator powerful enough to steer the wheel-robots and to move the steering axis to the center of the tire. Redesigning a half-scale model of the wheel-robot allows for testing of the vehicles functionality at a much lower cost compared to manufacturing a full-scale prototype of the CityCar. Due to the tight time schedule and budget, design options were constrained and it was advised to utilize parts already available in the Media Lab. Parts ordered needed to be cheap and quickly attainable, and newly designed pieces needed to be easily manufacturable within the Media Labs facilities. Because the design of the half-scale model is not actually scalable to a full-size vehicle, since motor size and power dont scale linearly, the intent of the model is to act more as a proof of concept than an actual final product design.

THIS PAGE INTENTIONALLY LEFT BLANK

Chapter 2

Smart Cities Group

2.1 Background

The Smart Cities Group at the MIT Media Lab has been working on an advanced urban improvement program that focuses on intelligent mobility and transportation. Professor William J. Mitchell, the director of Smart Cities, describes the group's research as focusing "upon intelligent, sustainable buildings, mobility systems, and cities. It explores the application of new technologies to enabling urban energy efficiency and sustainability, enhanced opportunity and equity, and cultural creativity" [8]. The group has three main mobility projects under simultaneous development: the GreenWheel, RoboScooter, and CityCar.

2.2 Current Mobility Projects

2.2.1 GreenWheel

The GreenWheel, as seen in Figure 2-1, is a standard rear bicycle wheel fitted with a custom designed hub system that contains batteries, a generator and an electric motor controlled from the bicycles handlebars. As the cyclist pedals, energy is stored in the hubs batteries, and can later be used to power the motor, driving the bicycle like a scooter. The GreenWheel can replace virtually any standard rear bicycle wheel.

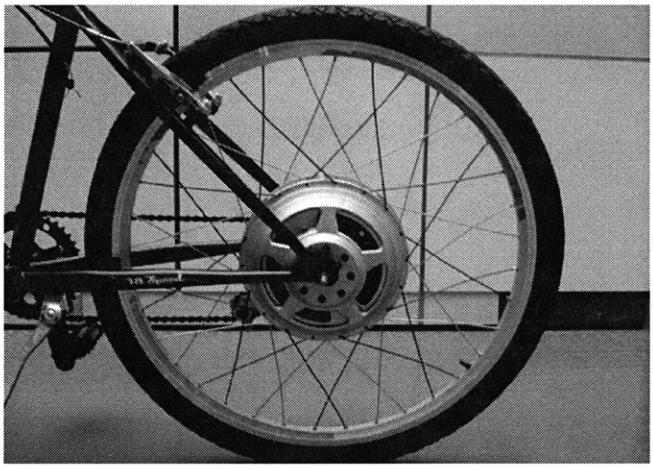

Figure 2-1: GreenWheel [7]

2.2.2 RoboScooter

The RoboScooter, as seen in Figure 2-2, is a shareable, foldable, lightweight, electric urban scooter. The project aims to reduce carbon emissions with its silent green scooter and cut down on parking congestion in dense urban areas around the world. Its folding feature is meant to allow for easy storage and to increase parking capacity at charging stations located in the urban environment.

Figure 2-2: RoboScooter [7]

2.2.3 CityCar

The CityCar, as seen in Figure 2-3, is a shareable, foldable, electric urban vehicle. The project aims to provide an alternative source of transportation in an urban environment. Like the ZipCar, the CityCar would be shared by the public and could be parked at one of the many charging stations located throughout the future the city. It folds upright, cutting its footprint in half, which in turn allows for more cars to be stacked next to each other within a confined space. All four wheels of the CityCar are electric-powered and independently controlled by an on-board CAN-BUS network.

Figure 2-3: CityCar [18]

THIS PAGE INTENTIONALLY LEFT BLANK

Chapter 3

Wheel-Robots

The CityCar, like any standard automobile, utilizes four maneuverable wheels: two in the front and two in the back of the car. The special functions of the CityCar are what make it different from the standard car in terms of wheel design.

3.1 Independently-Controlled Wheels

One of the functional requirements of the CityCar is the ability to fold in half, bringing the rear end towards the front as the carriage raises itself up [Figure 3-1a]. This is not feasible with the use of a standard automobile drive train [Figure 3-1b], which would interfere with the folding of the car. Therefore, the front and rear wheels need to be decoupled.

Another functional requirement of the vehicle is the ability to translate sideways. This requires rotating each wheel inwards toward the vehicle frame, which necessitates the decoupling of the left wheels from the right ones. In order to meet these two important functionalities, each wheel must be independently controlled and actuated, thus the term "wheel-robot."

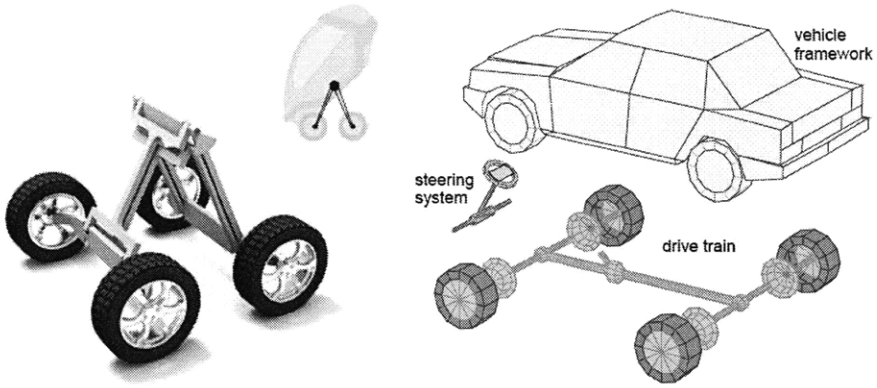

(a) Folding CityCar Frame [18] (b) Standard Drive Train [12]

Figure 3-1: Drive Train Comparison

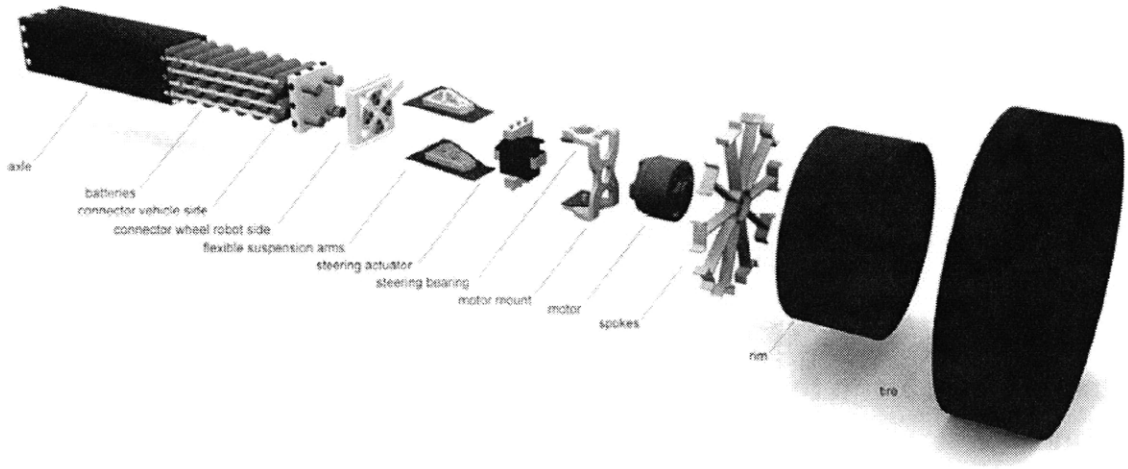

Figure 3-2: Wheel-Robot (Exploded view) [13]

As illustrated in Figure 3-2, the major components of a wheel-robot include the steering actuator, drive motor, suspension arm, and non-pneumatic tire. Since the City Car is meant to have a modular drive system, each wheel-robot is nearly identical in every way to allow for unlimited interchangeability between different CityCars in all four attachment locations. Each wheel-robot is self-contained, simplifying the process of repairing damages to certain components. The modularity of the wheel-robots allows them to be removed as a whole unit without the need to operate on the entire vehicle. Reconfigurable, self-contained and digitally controlled, the wheel-robots are very valuable and essential components to the Smart Cities CityCar.

3.2 Component Functional Requirements

3.2.1 Steering Motor

The steering of each wheel is unlike a typical automobiles. The CityCar is capable of omni-directional motion, made possible by its having four independently-controlled wheel-robots. Figure 3-3 illustrates the three main driving modes that the CityCar features: straight, zero-turn, and sideways.

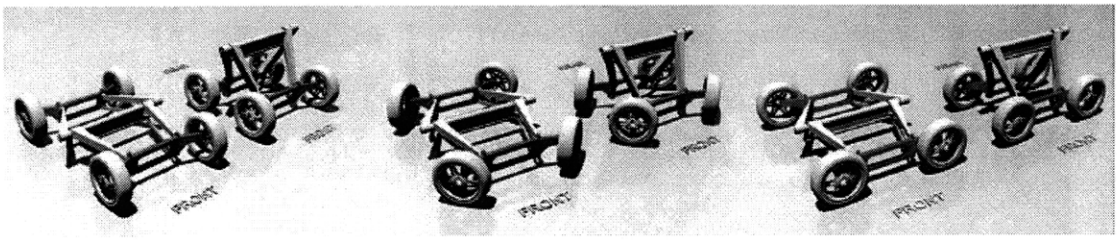

Figure 3-3: Wheel-Robot Driving Modes [13]

In order for the vehicle to achieve lateral movement, the wheels need to rotate inwards toward the car frame. The wheels also have to be able to pivot away from the car frame to able to round corners on the street. The steering motors therefore have to have sufficient torque to overcome the friction between the tires and the ground and also must be mounted in such a way as to not hinder the turning of the wheel as it spans its steering range.

Another requirement is that the steering not be back-drivable, thereby assuring that the vehicle will handle in a predictable and reliable manner.

3.2.2 Drive Motor

For each wheel to be independently driven while within the steering angle range, the driving motor must be embedded within the wheel. These in-wheel motors can therefore act as the wheels hub to eliminate the increase in weight and space consumption required by a separate drive motor and hub. For the half-scale prototype, the drive

motors also served as the braking source for the model, as this reduces the number of parts in the wheel-robot, simplifying the overall design.

3.2.3 Suspension System

Since all of the main driving components are to be integrated together, the wheel-robot needs to contain a suspension system independent from the rest of the vehicle. As with any car, the suspension needs to be capable of supporting the weight of the vehicle and its passengers and any additional sensible payload. It must prevent the lower surface of the CityCar from making contact with the ground and absorb a large amount of the energy while riding over obstacles.

3.2.4 Tires

As in a conventional automobile, the tires need to provide supplemental energy absorption while driving over small obstacles. Generally, pneumatic tires deform when making contacting with obstacles, cushioning the ride and providing an overall fluidic driving experience for the passengers. The CityCar would also need impact-absorbing tires to smooth out the ride.

Chapter 4

Schmitt's Half-Scale Prototype

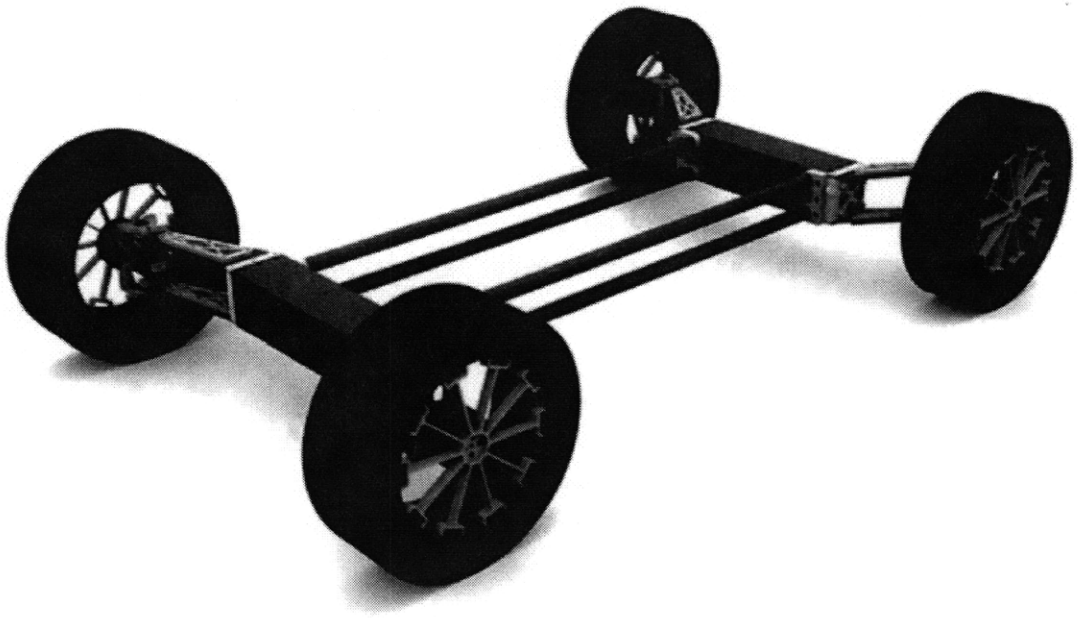

Figure 4-1: Schmitt's Half-Scale Wheel-Robots [13]

4.1 Steering

4.1.1 Steering Axis Location

Figure 4-1 shows Peter Schmitts half-scale prototype, which consists of four half-scale wheel-robots attached to a simple structural frame. As shown in Figure 4-2, each wheel-robots steering axis is offset a small distance, x_0, away from the wheels center of mass, toward the cars frame.

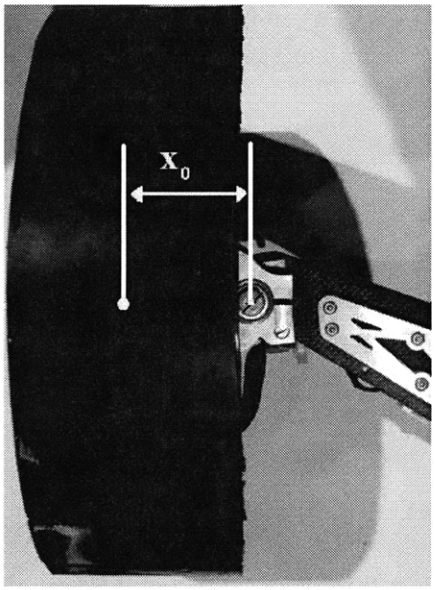

Figure 4-2: Offset Steering (Top View)

Having the steering axis offset from the wheels center of gravity is not an ideal design and causes problems with the cars steering ability. This aspect of the design was one of the main reasons for the decision to redesign the half-scale prototype.

4.1.2 Steering Actuator

Schmitts prototype makes use of a small servo motor, seen in Figure 4-3, as the steering actuator. While using a servo motor has the benefit of having built-in controls, it lacks sufficient torque needed to steer the wheel under the weight of the prototype.

Figure 4-3: Hi-Tech HSR-5995TG Servo [2]

It was clear that stronger actuators needed to be used in the redesigned prototype. The servo motors Schmitt uses are also easily back-drivable, which, as has already been mentioned, is not an ideal characteristic for a moving vehicle.

4.2 Driving

Figure 4-4: Scanner RC Brushless Outrunner Motor [1]

Schmitt's design uses a brushless, outrunner DC motor, similar to Figure 40, as his driving motor for the half-scale wheel-robots. Outrunners have a rotating magnet-lined outer casing, spinning around a wire-wound fixed stator. The motor used is lightweight and meant to power lightweight model airplanes.

4.3 Suspension

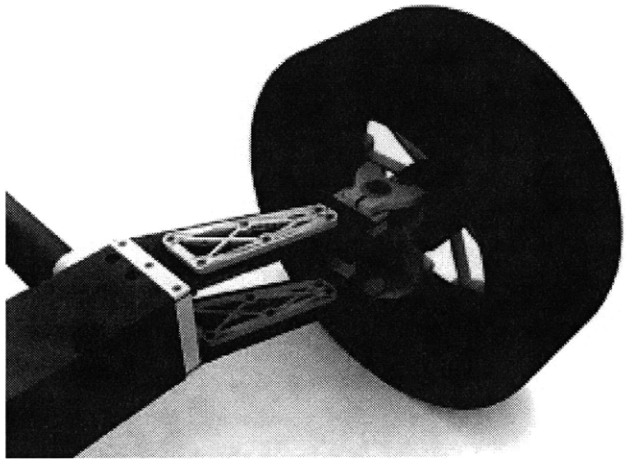

Figure 4-5: Schmitt's Flexural Suspension Arm [13]

Schmitts half-scale wheel-robot uses the connection arm, which connects the inside of a wheel-robot to its base, as the primary suspension component of the half-scale vehicle rather than using a complex in-wheel suspension as was proposed for earlier designs. This integration of the suspension into the physical arm that provides structural support for the wheel-robot is a novel idea. In such a system, the arm consists of a set of two carbon-reinforced, composite sheet flexures that performed as cantilever beams. This suspension concept is structural and therefore it was decided not to make a priority out of redesigning this component of the wheel-robot.

4.4 Tires

Schmitt wanted to incorporate a tire design inspired by the Tweel™, an innovative, non-pneumatic, experimental tire being developed by the Michelin®company. With its airless design, the Tweel™[Fig. 24] cannot burst or run flat. Its outer rim is supported by flexible polyurethane spokes that connect to the Tweel™hub and aide in shock-absorption. Each spoke is in tension, which is beneficial to the energy conservation as the Tweel™deforms in contact with the ground and other obstacles.

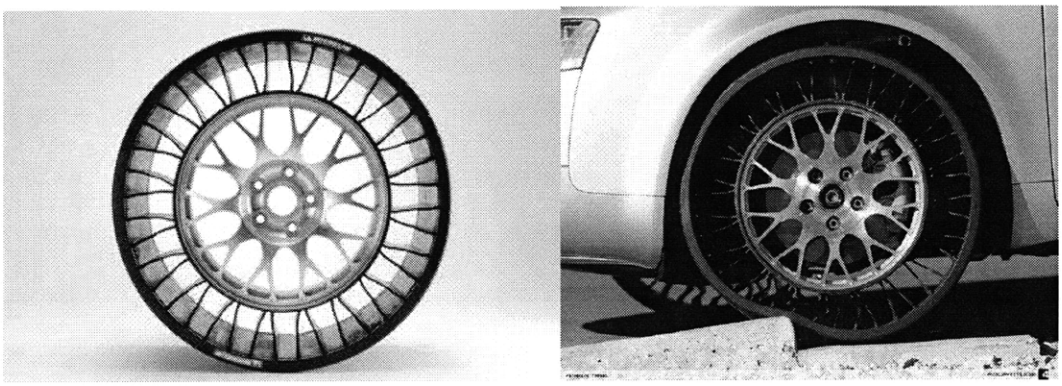

(a) Static (b) Driving Over Bump

Figure 4-6: Michelin®Tweel™(Front View)[11]

The deforming spokes allow for driving over imperfections in the road and over small obstacles, much like a pressurized tire full of air would. Seeing the Tweel™as the future of the modern day tire, Schmitt and the Smart Cities Group wanted to explore its technology for possible use with the CityCar.

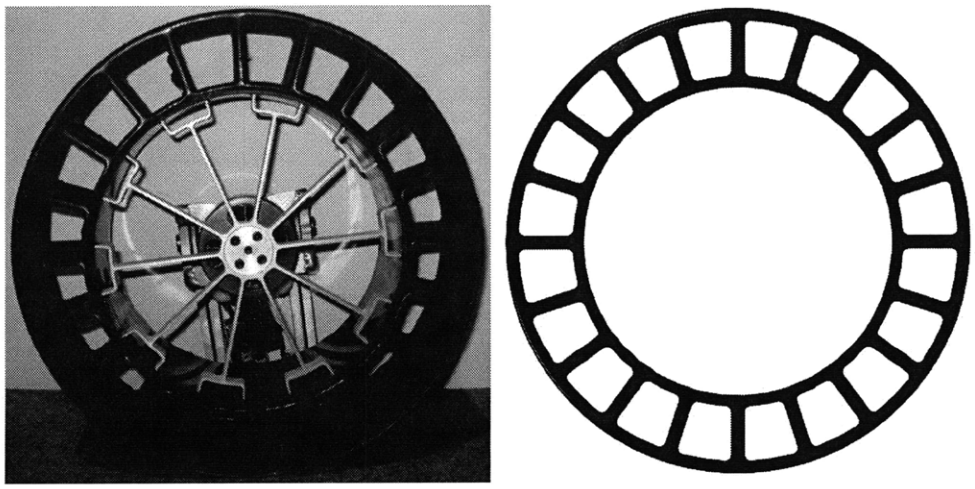

(a) Actual (Front View) (b) CAD (Front View)

Figure 4-7: Schmitt's Rubber Cast Tire

The difference between Tweel™technology and Schmitt's exploration is that Schmitts tires made for the half-scale prototype are simply cast out of synthetic urethane rubber, and its spokes lack the internal tension which is key to the Tweel™performance. Schmitt's half-scale tire hub is supported through compression of the spokes when the

tire deforms under the cars weight, much like the wooden spokes of a horse carriage from olden days. The Tweel™supports the hub through tension in the spokes. Because of this, Schmitts design does not actually utilize the main principle behind the Tweel™technology and its properties. Schmitt's tire design [Fig. 12] also makes use of a stiff cylindrical rim as a structural component of the tire. Schmitt's design was interesting and deserved further investigation, but redesigning it was not a priority.

Chapter 5

Half-Scale Wheel-Robot Redesign

5.1 Steering

5.1.1 Steering Axis Location

Having the steering axis offset by x_0, as seen in Figure 4-2, results in the friction force between the tire and the ground acting against the driver. The friction force applies an additional torque about the steering axis, even when the wheel is pointed forward and the car is trying drive in a straight line. As Equation 5.1 shows, the greater x_0 becomes, the larger the frictional moment, M_f, acting about the steering axis becomes.

$$M_f = x_0 \times F_f \tag{5.1}$$

If the steering actuator cannot provide enough torque to counteract M_f, then the entire wheel will rotate around the steering axis when the vehicle is trying to drive forward or backward, as in Figure 5-1a. The consequences of such lack of handling are obviously undesirable. Another downside to having the steering axis offset from

the center of the wheel is that the total working volume of the wheel-robot increases. Since the tire is offset from the axis about which it rotates, then as the wheel steers clockwise relative to the axis, its body spans a larger workspace volume. This large steering volume is illustrated in Figure 5-1b, where the steering axis is marked by the cross-hair.

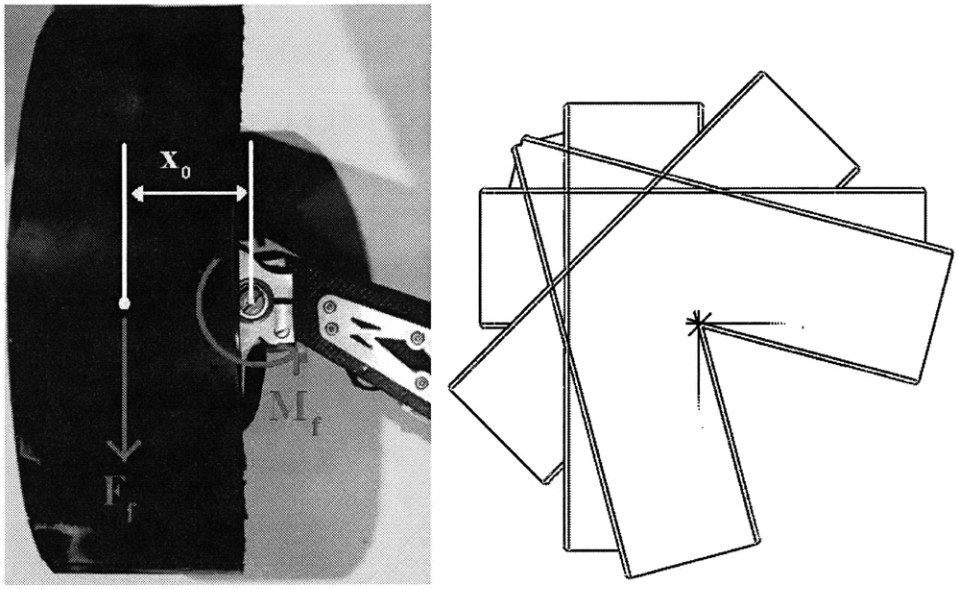

(a) Frictional Moment (b) Offset Steering Volume

Figure 5-1: Offset Steering Axis Problems

By having the steering axis pass through the center of the wheel-robot tire, two main benefits emerge. First, having the wheels steer about their tires contact point with the ground allows the wheels center of mass to remain stationary relative to the cars frame, keeping the wheel within a spherical volume as it steers, as seen in Figure 5-2b. This steering workspace is smaller than the one in Figure 5-1b, keeping the overall size of the CityCar to a minimum. Secondly, decreasing the steering axis offset distance to zero avoids the need for a stronger, and most likely larger, steering actuator. Since the design of the wheel-robot has space constraints, larger components are highly undesirable.

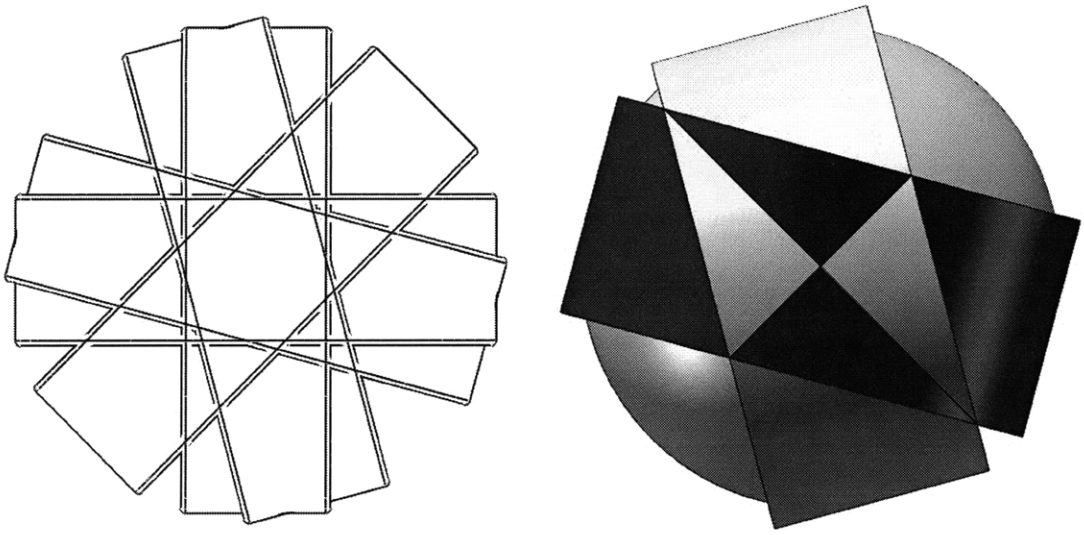

(a) Tire Movement (b) Steering Volume

Figure 5-2: Optimal Steering Volume

5.1.2 Preventing Back-Driven Motion

The servo motors Schmitt uses in his half-scale prototype are not only too weak to power the steering of a fully-equipped half-scale CityCar, they are also easily back-drivable. That means the wheel-robots could easily be forced out of alignment with each other. Part of the redesign meant finding a stronger motor to serve as the steering actuator and to figure out a way to prevent the steering from being back-driven.

In order to prevent the steering actuators from being back-driven, a mechanical stop needed to be utilized. The weakness in back-drivable systems is that the motor or actuator needs to constantly be exerting a force to prevent loads from causing unwanted motion in the system. A simple solution to this problem is implementing a screw drive design, as shown in Figure 5-3a. A linear screw drive design is one that has a non-rotating carriage riding on a stationary threaded rod that is spinning about its axis. As the threaded rod spins, the rotation constraint on the carriage forces it to translate along the shafts length. However, if a axial load is placed on the carriage, in the direction of the threaded rod's axis, then the rod's teeth take the load, but the carriage does not travel down the rod. Only a rotation from the threaded shaft can

linearly translate the carriage. This feature is comes in handy when vertical motion is desired without having to worry about the carriage falling back down under its own weight. In the case of a vertical threaded rod drive system, the weight of the carriage is supported by the threads when the shaft motor is turned off and therefore this system doesnt require the motor to be on constantly.

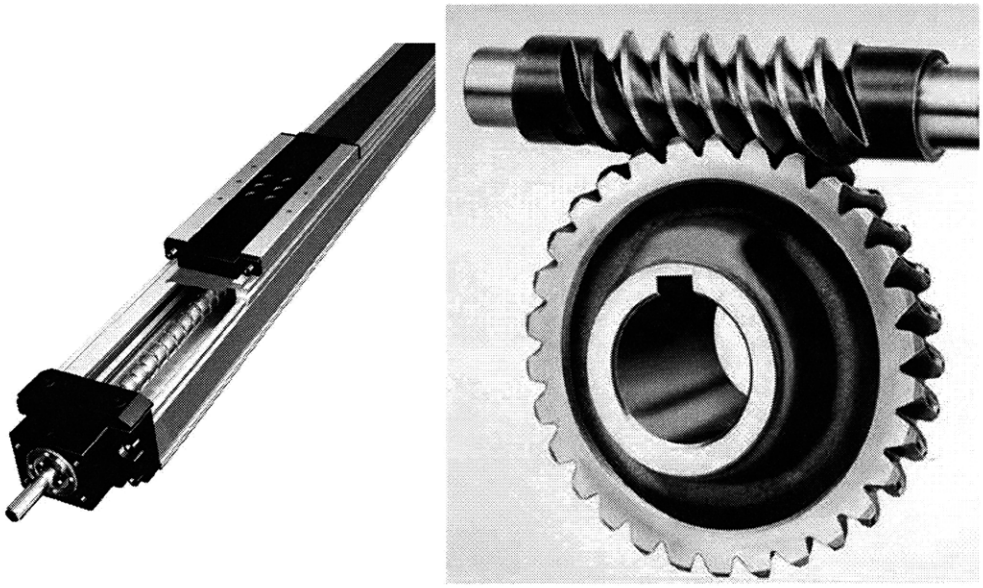

(a) Linear Screw Drive System [15] (b) Rotary Screw Drive System [9]

Figure 5-3: Screw Drive Systems

The same idea can be applied to a rotational screw drive system, seen in Figure 5-3b. As the threaded shaft, called a worm gear, rotates, its threads apply a force on the teeth of the sun gear, causing the sun gear to spin about its axis. When the worm gear stops turning, the sun gear effectively comes to a stop and will remain in that position. Backlash between the sun gear teeth and the worm gear would allow small, near-negligible rotational play in the sun gear. Aside from the minor backlash, applying a tangential load to the sun gears teeth would in turn apply an axial load on the worm gear in the direction of the shafts length. Since this is a linear force acting on the worm gear teeth, the worm will not rotate about its axis and therefore the sun gear cannot move. It is effectively stuck in the position the worm gear left it in. This method was chosen to use in the steering system to prevent the wheels from turning undesirably due to external forces. Ideally, the axis of the sun gear would be

collinear with the tires center of mass.

5.1.3 Determining Steering Torque

In order to design a functional half-scale wheel-robot, the required steering torque needed to be calculated. In a standard vehicle, the geometric center of each tire is stationary relative to the car frame, as shown in Figure 3-1b. A standard pneumatic tire, of outer diameter d_w and width t_w, compresses a small amount when it contacts the ground [Figure 5-4a], creating a contact patch against the ground, as seen in Figure 5-4b.

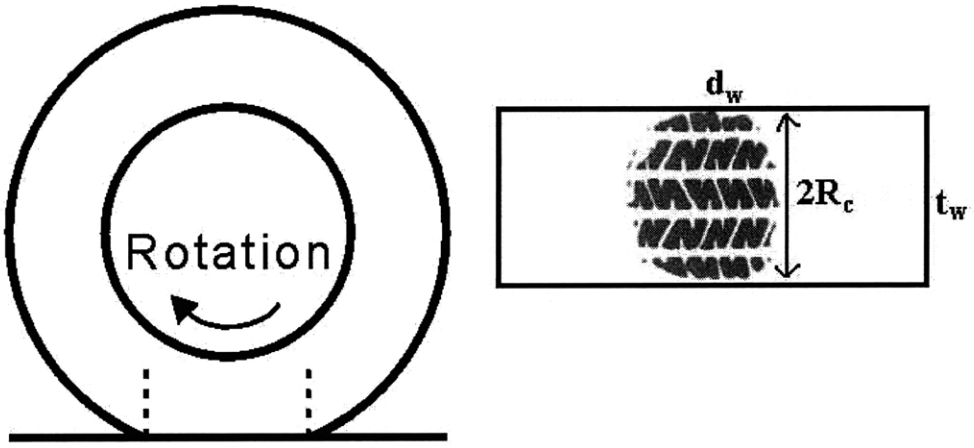

(a) Compressed Tire [6] (b) Contact Patch

Figure 5-4: Tire Contact Geometry

When a vehicle makes a turn, each wheel pivots about the center of its contact patch. In a simple model, W, the weight of the vehicle and its passengers, is distributed equally to all four wheels. Therefore, the normal reaction force, F_N, acting up on each wheel is equal to one quarter of the total weight acting on the vehicle. As a wheel-robot pivots, a frictional force, F_f, is generated between the tire and the ground.

$$F_f = \mu_s \times F_N = \mu_s \times \frac{W}{4} \tag{5.2}$$

In Equation 5.2, μ_s is the coefficient of static friction between the tire and the ground. The frictional force generated acts on the entire contact patch, and in order for the tire to pivot about the patchs center, the frictional moment acting on the patch must be overcome.

To estimate this frictional moment, the contact patch area had to be estimated. Assuming a flat contact surface, the contact patch, shown in Figure 5-4b, was modeled as a flat circle of radius R_c. It was assumed that the circular contact patch spanned the entire width of the tire and therefore,

$$t_w = 2 \cdot R_c. \tag{5.3}$$

The contact pressure, P, acting on the contact patch was assumed to be uniform for the steering torque calculation and is defined in Equation 5.4.

$$P = \frac{F_N}{A_c} = \frac{W/4}{\pi R_c^2} = \frac{W}{4\pi R_c^2} \tag{5.4}$$

Using Equation 5.1 and taking the frictional moment about the center of the circular contact patch described in Figure 5-4b, a steering torque requirement can be calculated by integrating over the entire contact area. The moment arm, r, is measured radially outward from the center of the contact patch. As Equation 5.6 shows, dA_c can be rewritten in polar coordinates.

$$d\tau_s = r \cdot \mu_s \cdot P \cdot dA_c \tag{5.5}$$

$$dA_c = r \cdot dr \cdot d\theta \tag{5.6}$$

Substituting Equation 5.6 into Equation 5.5 allows for integration across the area of the contact patch, A_c.

$$\tau_s = \int d\tau_s = \mu_s \cdot P \int_a^b \int_c^d r^2 \cdot dr \cdot d\theta, [a,b] = [0, 2\pi], [c,d] = [0, R_c] \tag{5.7}$$

$$\tau_s = \frac{2\mu_s \cdot \pi R_c^3}{3} \cdot P \tag{5.8}$$

Substituting Equation 5.3 and Equation 5.4 into Equation 5.8 results in the final calculation for the steering torque requirement, τ_s, in Equation 5.9.

$$\tau_s = \frac{\mu_s \cdot t_w \cdot W}{12} \tag{5.9}$$

Table 5.1 contains the relevant parameter values for the half-scale CityCar needed to calculate the resultant required steering torque. The tire width, t_w, was set to be around half the width of a standard, full-scale tire for a compact car. Because the half-scale CityCar prototype halved all three axes of dimensions, it is only one-eighth the volumetric size of the full-scale CityCar, assuming consistent densities of all the materials. Therefore, the half-scale weight is one-eighth of the full-scales, which was estimated to be around 1000 lbs. As a safety factor, the calculated torque requirement, τ_s, was doubled to help ensure that the chosen steering motors would be strong enough to steer the wheels under extra loading.

As Table 5.1 shows, the minimum required torque needed from each steering actuator is 3.7 N-m. The Hi-Tech HSR-5999TG servo motor Schmitt uses in his half-scale wheel-robot has a maximum output torque of 417 in-oz (2.95 N-m), which explains

Table 5.1: Half Scale Wheel-Robot Steering Torque

spanning example				
μ_s	t_w (in)	W (lbs)	τ_s (N-m)	$2\tau_s$ (N-m)
0.9	3.5	125	3.7	7.4

why his wheel-robots were not able to steer under the weight of his incomplete, half-scale prototype [2]. The servos were not capable of providing enough torque to overcome the frictional moments acting on each wheel's contact patch.

5.1.4 Steering Actuator Selection

With the required steering torque calculated, the next move was to find a suitable motor capable of meeting the desired performance requirements. Due to time and budget constraints, the choice was limited by the cost of the motor and the speed at which it could be obtained.

To implement a worm-sun gear mesh independently would have cost the design group time as well as increase the number of parts needed for assembly, which complicates the design. Therefore, it was decided that a pre-fabricated worm-sun gear mesh system would be purchased from outside sources. Early ideas involved buying a worm-sun gear gearbox to couple with the steering motor, but attempts at finding a small enough gearbox were unsuccessful. Figure 5-5 depicts one of the gearboxes considered.

While searching for more gearboxes, motors with a worm-sun gear mesh built into the housings were discovered. This provided two benefits as it minimized the size of the overall, low back-lash system and saved manufacturing time needed in making an in-house gearbox. A reliable provider of these motors was found and a motor was chosen based on its motor characteristics and documented performance.

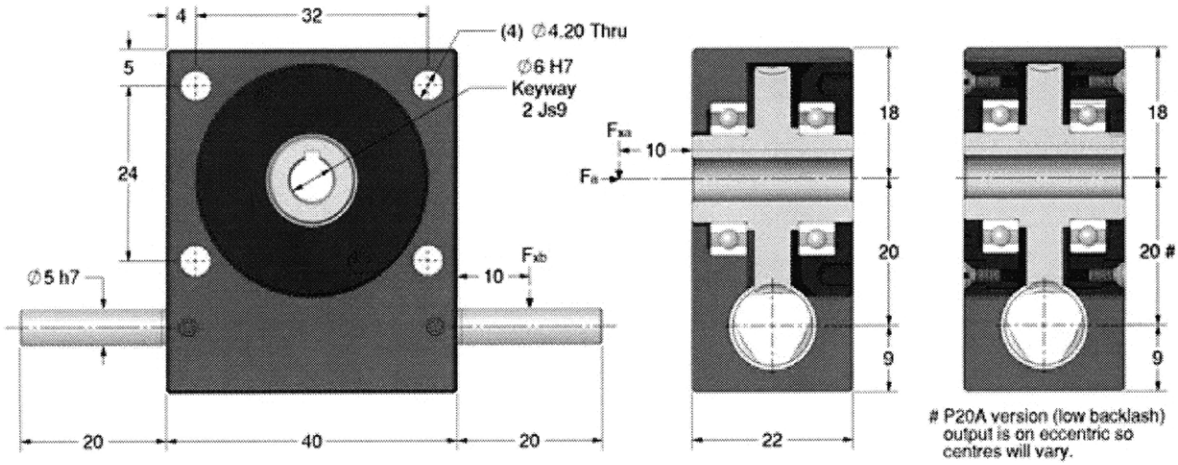

Figure 5-5: Worm-Sun Gearbox [10]

Motor Characteristics

The rotational speed of the output shaft of a motor is directly proportional to the amount of loading torque applied to it. Figure fig:5-aspect4b illustrates the linear relationship between the rotational speed of the shaft, ω, and the output torque, τ. The maximum torque a regular DC (direct current) brushed motor can output is its stall torque, τ_0, which causes the output shaft rotational speed to drop to zero. When there is no torque load on the output shaft, the shaft spins at its maximum speed, ω_0, called the no-load speed.

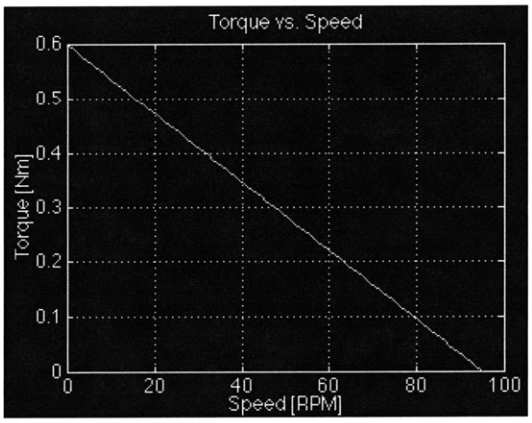

Figure 5-6: Example Torque-Speed Curve [3]

Equation 5.10 describes how to calculate the power output of a motor. Because of the linear relationship between torque and angular speed, the maximum power output

comes when a motor is run at half the no-load speed, as Figure 5-7 depicts. The stall torque is a characteristic of a motor, and is defined by the torque required to stall the output shaft, making its rotational velocity equal to zero. When the motor stalls out at the stall torque, its power output is zero because the output speed is at a zero value. Zero power is also achieved when no torque load is applied to the shaft as it spins at its no-load speed.

$$P_m = \tau \cdot \omega \tag{5.10}$$

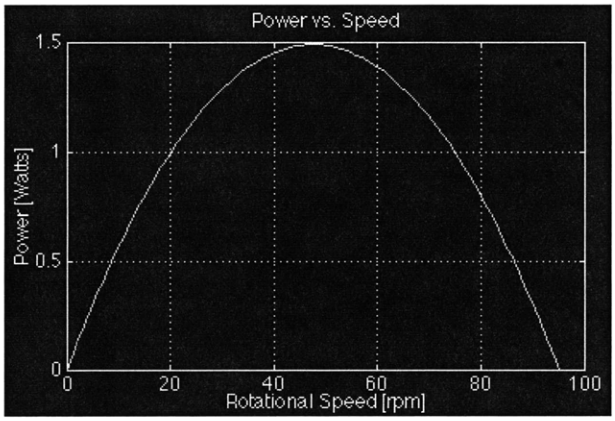

Figure 5-7: Example Power-Speed Curve [3]

Motor efficiency, η_m, as defined by Equation 5.11, is the ratio between the mechanical power output of the motor and its electrical power input. An ideal motor would convert all of its electrical power, P_e, into pure mechanical motor power, P_m, having an efficiency value of 1, making it 100 percent efficient.

$$\eta_m = \frac{P_m}{P_e} \leq 1 \tag{5.11}$$

AME Worm-Gear Drive

The decision was made to use a motor originally designed to lift car windows and was originally manufactured by AM Equipment. The AME 210 Series 10 N-m 12-Volt

motor was chosen for its small packaging, built-in worm-sun gear transmission, and ability to be used as the steering actuator for the half-scale wheel-robot. Figure 5-8 depicts the torque-speed curves for this particular motor when it is driven at its 12 volt rating. Figure 5-9 provides motor data for when the motor is driven in both the counter-clockwise and clockwise direction.

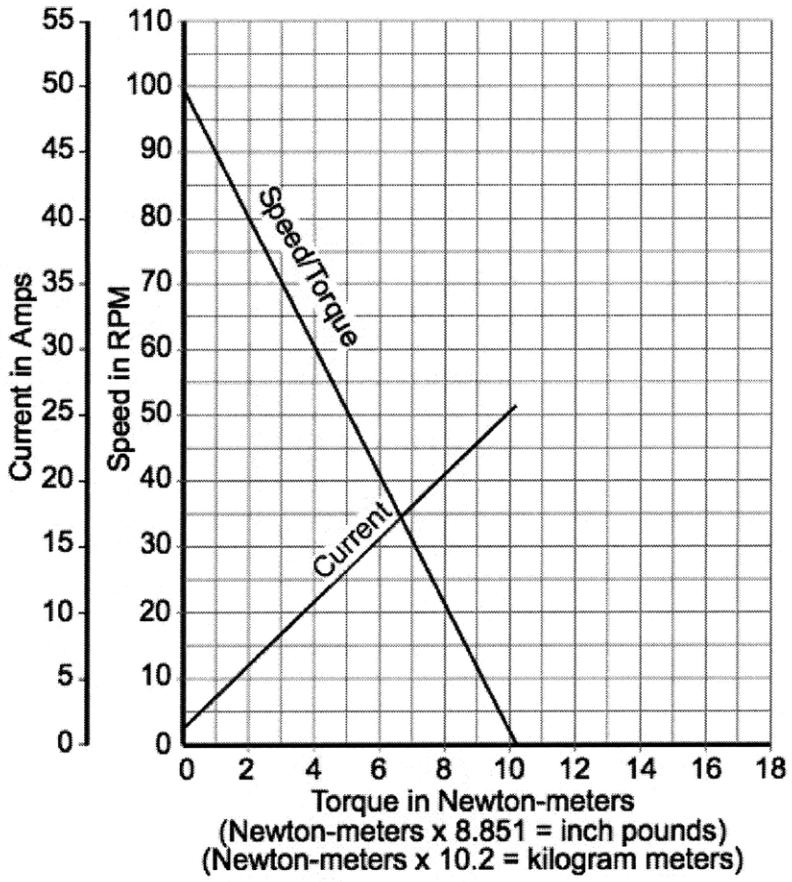

Figure 5-8: AME 10 N-m Motor Torque-Speed Curve [4]

According to Figure 5-9, the AME motor reaches its peak power at a rotational speed of roughly half that of its no-load speed, as expected. Nominal operating torque of 3.1 N-m (for counter-clockwise direction), which falls short of the required steering torque of about 7.5 N-m. To make up for this, a gear reduction of 3:1 is to be introduced, tripling the performance torque to 9.3 N-m, which is above what is needed. But introducing the gear ratio in turn reduces the nominal operating speed by one-third, bringing ω down to roughly 20 rpm.

Counter-Clockwise Motor Shaft Rotation		
Data Point	Data Type	Value Range
No Load	Current (A)	3.5 - 2.9
	Speed (rpm)	108.0 - 88.5
Stall Load	Torque (Nm)	11.2 - 9.2
	Current (A)	26.9 - 22.0
Peak Power	Power (W)	29.1 - 23.8
	Torque (Nm)	6.1 - 4.9
Nominal (Peak Efficiency)	Power (W)	21.2 nominal
	Speed (rpm)	67.4 nominal
	Current (A)	8.8 nominal
	Torque (Nm)	3.1 nominal
Clockwise Motor Shaft Rotation		
Data Point	Data Type	Value Range
No Load	Current (A)	3.8 - 3.0
	Speed (rpm)	106.2 - 86.9
Stall Load	Torque (Nm)	11.0 - 9.0
	Current (A)	28.0 - 22.9
Peak Power	Power (W)	30.9 - 25.3
	Torque (Nm)	5.6 - 4.6
Nominal (Peak Efficiency)	Power (W)	24.2 nominal
	Speed (rpm)	70.1 nominal
	Current (A)	9.2 nominal
	Torque (Nm)	3.4 nominal

Figure 5-9: AME 10 N-m Motor Info Table [4]

$$V = k_m \cdot \omega \tag{5.12}$$

A functional requirement of the steering is that the wheel must be able to pivot at a minimum of 1 revolution per second, which translates to 60 rpm. Therefore, the nominal operating speed needs to be increased without lowering the new nominal operating torque of 9.3 N-m. Shaft rotational speed is directly proportional to the applied voltage, as shown in Equation 5.12, where k_m is the motor constant. Therefore, tripling the operating voltage from 12V up to 36V triples the output speed back to its original nominal value of around 67 rpm. The reason for achieving these operating conditions is due to the fact that the CityCar will be running on a 36V system, and therefore having the steering motor be operable around that voltage would be a desirable characteristic. Figure 5-10 and Figure 5-11 both illustrate the AME motor

that was chosen based on its power output capabilities and pricing. Choosing this AME motor minimized cost and space consumption, both of which were valuable to the design process.

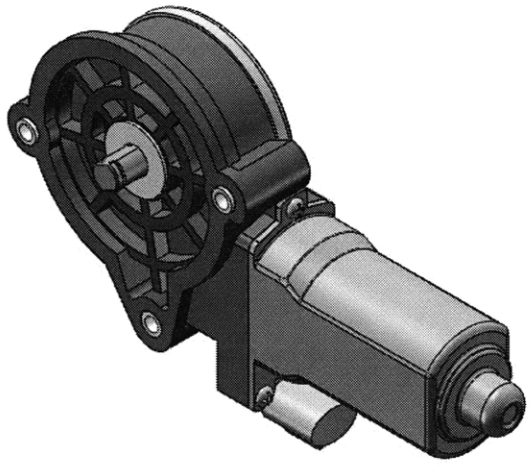

Figure 5-10: AME 10 N-m Motor (Isometric View) [4]

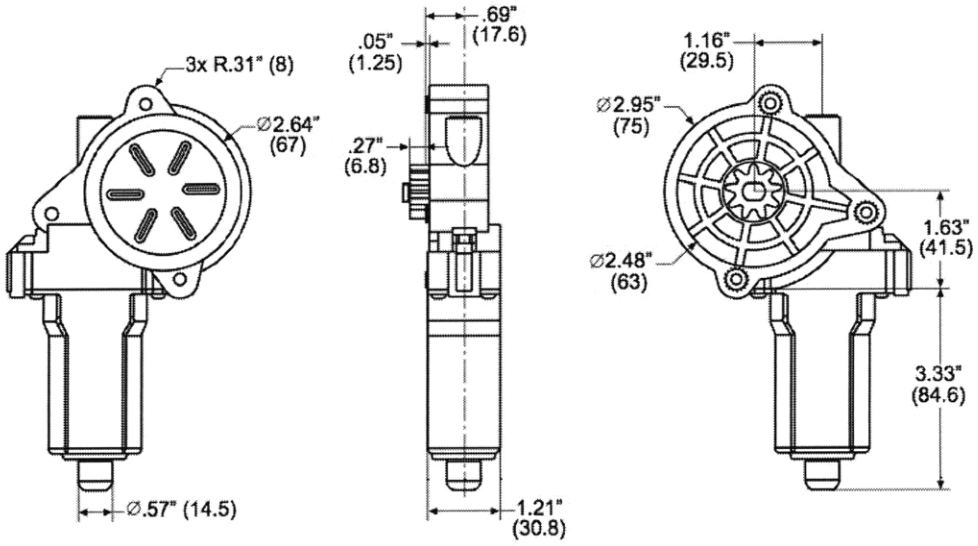

Figure 5-11: AME 10 N-m Motor Dimensions [4]

5.2 Driving

Since the half-scale CityCar prototype weighs approximately 125 lbs ($m \approx 57$ kg), there was a concern about whether the lightweight motor could handle the load. Schmitt's half-scale prototype didnt include the entire CityCar assembly - it simply had a structural frame for the wheel-robots to connect to - and so Schmitt did not have to take into account the final weight of the vehicle in his design.

A decision was made to replace the half-scale drive motor with a larger, more powerful motor that would more closely resemble the motor that might eventually be used in the full-scale version of the CityCar. Figure 5-12 depicts the 36V motor chosen to replace the lightweight motor used in Schmitt's prototype.

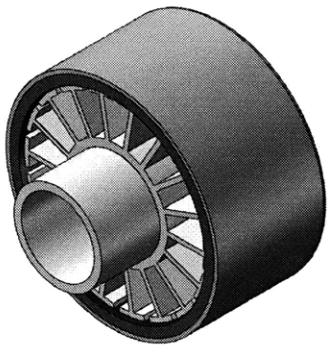

Figure 5-12: New 1000W 36V Brushless Outrunner Drive Motor

Figure 5-13 provides an exploded view of the main components of the drive motor that was chosen. The motor consists of two main parts: (i) the inner stator containing the wire windings, and (ii) the outer casing that has a magnetic ring adhered to its inner cylindrical wall.

Due to the fact that the chosen drive motor had an outrunner design, meaning the outer casing could be used as the rotating part while the stator remained fixed, it was decided to use the outer casing as the hub of the wheel-robot. Metal spokes would rest on the outer casing hub and support the inner diameter of the rubber cast tire. Figure 5-14 provides relevant dimensions of the chosen drive motor.

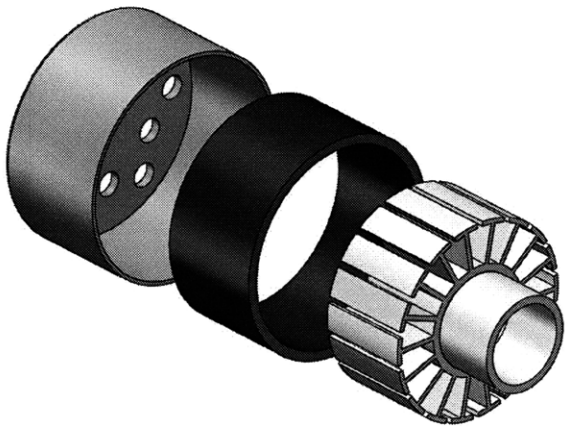

Figure 5-13: New Drive Motor Assembly (Exploded View)

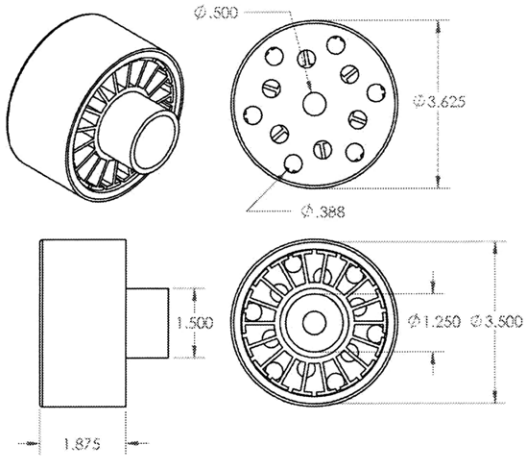

Figure 5-14: New Drive Motor Dimensions

5.3 Suspension

While it has already been stated that re-designing the wheel-robot suspension is not a priority for this design project, some thought has been given to the topic. In Schmitts system, the arm consists of a set of two carbon-reinforced, composite sheet flexures that performed as cantilever beams.

In conventional automobile suspension systems, a linear coil compression spring is used in parallel with a linear dashpot coaxially aligned with the spring, as shown in Figure 5-15a and Figure 5-15b. This pair act as a secondary connection arm, referred to as the wishbone link. One end of the system is attached to a pivot point on the

car frame and the other end is attached to the main connection arm, much like the configuration in Figure 5-15c. As the wheel drives over a bump or small obstacle, the connection arm pivots upward, axially compressing the spring and dashpot combo simultaneously. The larger the obstacle, the less the impact force is directed axially onto the spring and dashpot.

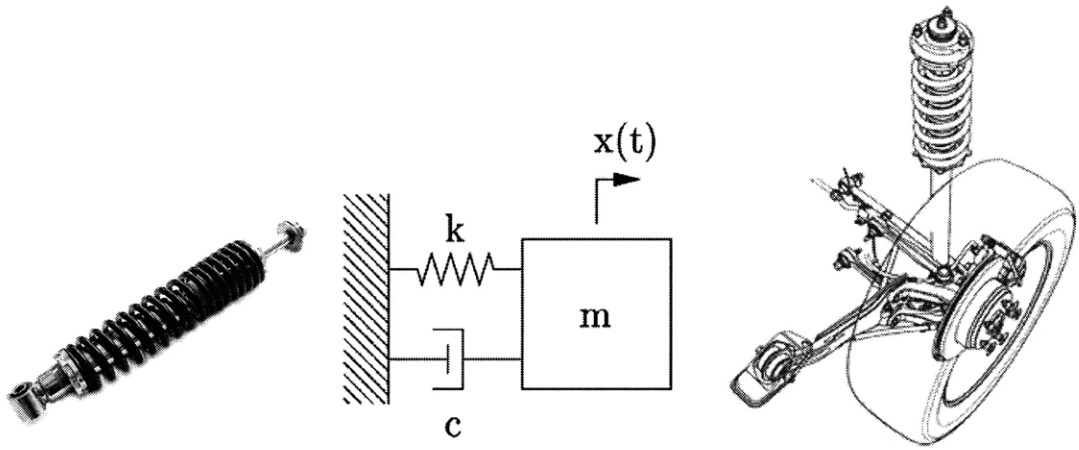

(a) Spring/Damper [17] (b) Dynamic Model (c) Honda Suspensions [16]

Figure 5-15: Conventional Suspension System

One idea that was discussed involved the use of a torsional spring and rotational damper in place of the conventional linear spring and linear damper. Both the torsional spring and rotational damper could be placed in such a way so that they share the same pivot axis as the base of the connection arm. In this design, there is no need for a secondary wishbone arm that connects to the main connection arm. This design also provides a reliable constant spring constant and torsional damping constant as the wheel drives over obstacles and bumps.

5.4 Tires

Schmitt's Tweel^{TM}-inspired tire design was doomed to never perform as well as the Tweel^{TM}, but it was successful in having partially similar behavior when under normal loading conditions. Figure 5-16a shows how the tire deforms under vertical loading.

The outer band of Schmitt's tire surrounds the 20 compressible spokes. When each section of the outer band that is located between spokes makes contact with the ground, it acts similarly to a simply-supported beam under mid-span three-point bending [Figure 5-16b], only that the pinned supports arent grounded and are actually buckling columns.

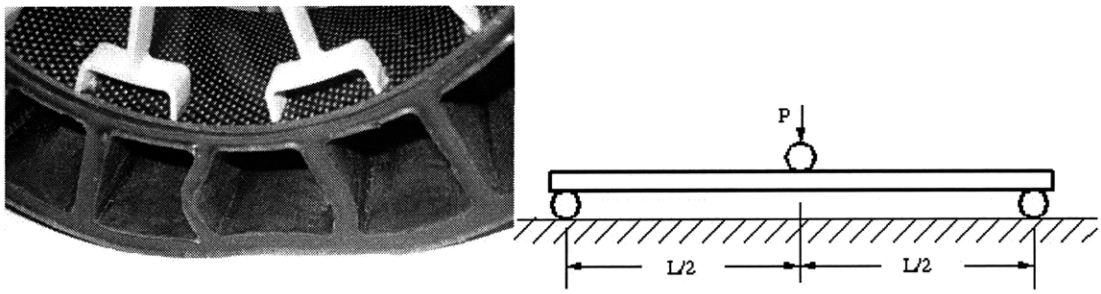

(a) Schmitt's Tire Deforming (b) Beam Under Mid-Span 3PB

Figure 5-16: Half-Scale Tire Deformation

The problem with this design is that when the tire is standing on top of a single spoke, the tire does not deform as much as it would if standing on a point between spokes. The reason for this is the natural stiffness of the cast rubber spokes. It takes much more energy to cause the spoke to buckle under the vehicles weight then it does to bend the strip of outer band located between two spoke ends, which was made clear by simply pushing down on the inside rim of the tire at different spoke orientations. The stiffness of the spokes causes inconsistent deformations in the tire as it rolls along the ground, which results in a bumpy ride.

In an attempt to even out the deformations and displacements caused by the normal force, F_N, acting on each tire, it was proposed that the spoke design be re-imagined. Schmitt had designed and fabricated a custom mold for casting the rubber mixture. He used a urethane rubber mixture produced by Smooth-On, a liquid rubbers and plastics company. Since Schmitt's original tire mold was still available for use, the only thing needed for different spoke designs was the interior components of the mold that could be made out of 3D printed parts. Three different designs were considered.

5.4.1 Rubber Spoke Concept 1

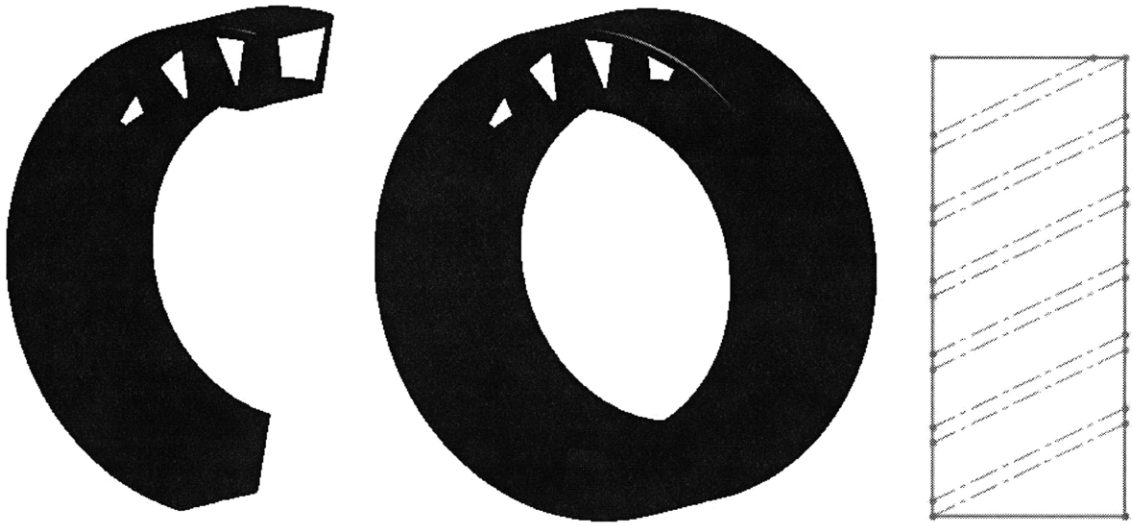

(a) Cross-Section (b) Isometric View (c) Top View

Figure 5-17: Twisted Spoke Concept Tire

In this design the spoke walls are slanted at an angle, as seen in Figure 5-18a. The slanted angle causes the end of one spoke wall to line up with the beginning of the next spoke. This provides a more distributed design since the spokes effectively covers the entire outer lateral surface of the tire. It would be easy to manufacture this design by replacing Schmitt's right-side up removable pillars used inside his mold with slightly slanted ones that following the curve of the empty spaces in the design. To remove the rubber tire upon curing, the tire would just need to be pulled in a constant, upward spiraling motion, following the shape of the spiraling pillars.

The downside to this design is that the tire is more stiff overall and therefore does not perform as much as Schmitt's tire. The tire stiffness increased because the tight spacing of the angled spokes caused the spokes to effectively act everywhere around the tire, leaving no portions of the outer rim free to deform.

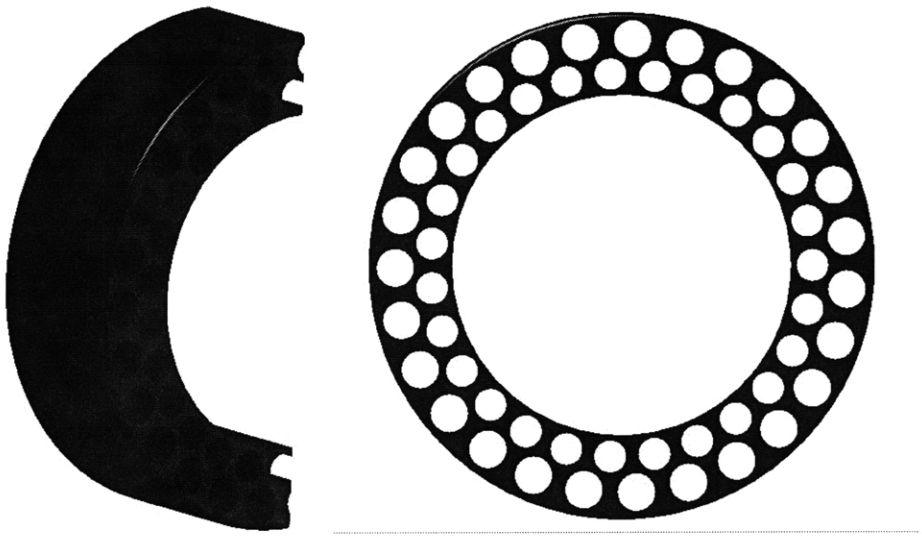

(a) Cross-Section (b) Front View

Figure 5-18: Circular Holes Concept Tire

5.4.2 Rubber Spoke Concept 2

These spokes were designed to be formed by using two concentric layers of circular pillars in Schmitt's mold. Having the bi-layer of holes allows for deformation in the inner layer in areas under the spokes located in the outer layer. This provides a more evenly distributed deflection since the spokes effectively no longer act as a source of high stiffness relative to the open-air portions of the tire design.

The downside to this design is that, since the open-air portions are cylindrical, it calls for roughly 4x the number of upright pillars to be installed into Schmitt's mold than did the original design. Due to the high cost of using the 3D printer, it iss not feasible to expect the group to spend 4x as much funds to test this design.

5.4.3 Rubber Spoke Concept 3

With this design there again exists two concentric layers of holes running through the tires thickness. This design was intended to improve on Design 2's idea of allowable deflection for all contact points along the outer lateral surface. A problem with Design

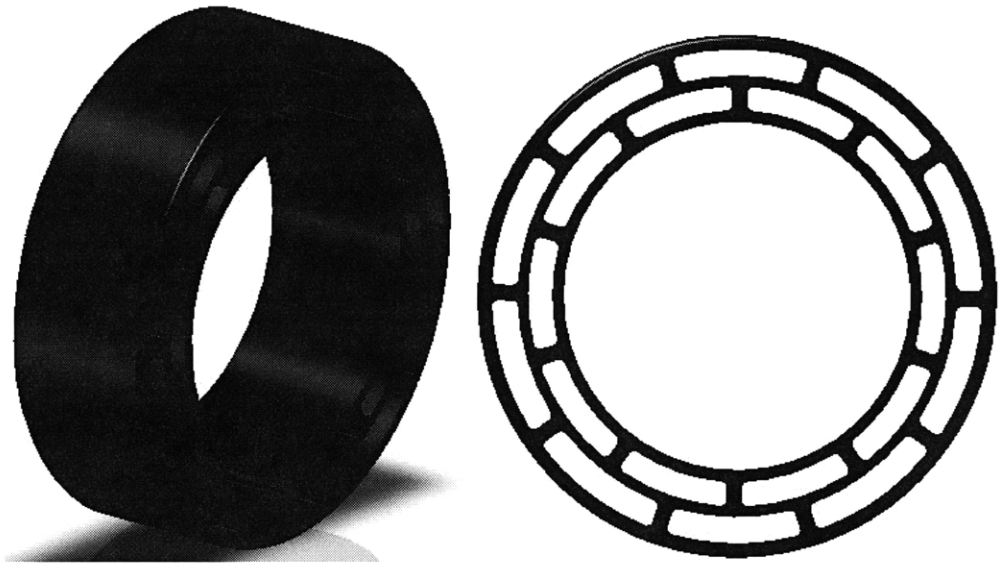

(a) Isometric View (b) Front View

Figure 5-19: Dual Spoke Layer Concept Tire

2's layout was in the unequal diameters of the cylindrical holes, leading to unbalanced deformations between the outer and inner layers.

Design 3 hoped to fix that by having near-identical holes in both of the concentric layers, as illustrated in Figure 93. This way, when the wheel is standing on a spoke located on the outer layer, the inner layer will deflect just above the top of that spoke. Likewise, when the wheel is standing on an outer layer space just between two spokes, then that strip of material on the outer layer will deflect inwards towards the tire's center. This design would also be easy to manufacture by replacing Schmitt's removable pillars used inside his mold with slightly wider ones. The number of pillars needed for Design 3 is 20, just like in Schmitt's original design, but here only 10 are needed per layer.

Chapter 6

Component Integration

6.1 Benchmarking

With the new steering and drive motors chosen, integration of all the wheel-robot components was the next step in the design process. The main concern was the ability to fit everything within the constrained space allotted for each wheel-robot. The CityCar used the well-known Smart®Car, featured in Figure 6-1a and Figure 6-1b, as a benchmark for its size and speed performance [14].

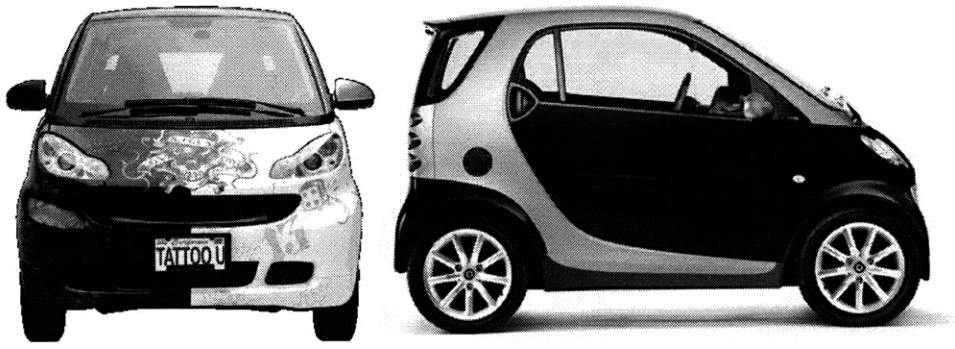

(a) Front View (b) Side View

Figure 6-1: Smart®Car [14]

The CityCar was modeled to have track width and wheelbase dimensions similar to

those of the Smart®Car. A vehicles track width is the distance between the center points of the left and right wheels, and its wheelbase is the distance between the center points of the front and rear wheels. Figure 6-2 shows the half-scale CityCar's track width and wheelbase to be 25.25 inches and 36.75 inches, respectively. These dimensions are half the Smart®Car's dimensions [14].

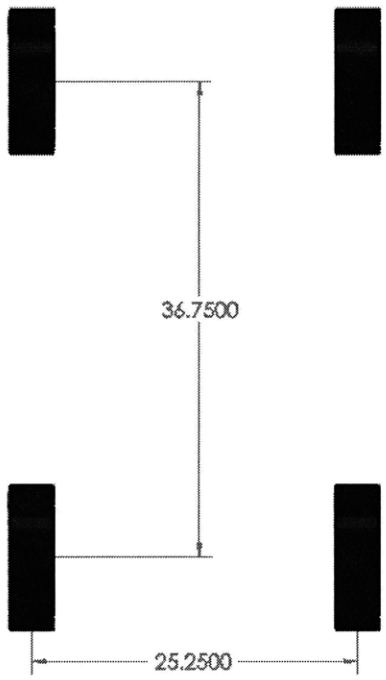

Figure 6-2: Half-Scale Track Width and Wheelbase

6.2 Steering Volume

Since one of the functional requirements of the wheel-robot is to have omnidirectional driving capabilities, the range of steering angles is quite large. In order for the CityCar to have the same maneuverability as a common compact vehicle, its front left wheel must also be able to turn roughly 15 degrees counterclockwise away from its initial position parallel to the side of the car. Another functional requirement of the CityCar is the ability to drive sideways, which requires all four wheels to pivot inwards. This means the front left wheel must be able to make a steer clockwise by right-angle turn

clockwise. As a safety factor, it was decided to allow the wheel to turn inward an additional 15 degrees beyond the right-angle inward turning angle. This results in a wheel-robot having a full steering range of 120 degrees (15 + 90 + 15 = 120 degrees).

Combining these two functionalities provides the working range of each wheel. Figure 5-2b shows a top-view perspective of both the steering angle range and how that illustrates the working volume that the tire uses up as it pivots about the center of the contact patch. This working volume was created by spinning the inside diameter of the tire around the ideal steering axis by 120 degrees. This working range provides a visual reference for how much space is open for the connection arm to reach into. The connection arm connects the base of the wheel-robot to the components that attach to the wheels geometric center. Figure 6-3 illustrates the slit of space left open after a tire has covered its entire span of motion. The image peers at the slit dead on, from a level position, and the red space is the inside surface of the tires. This undisturbed opening is the portal for the connection arm to make contact with the tires geometric center.

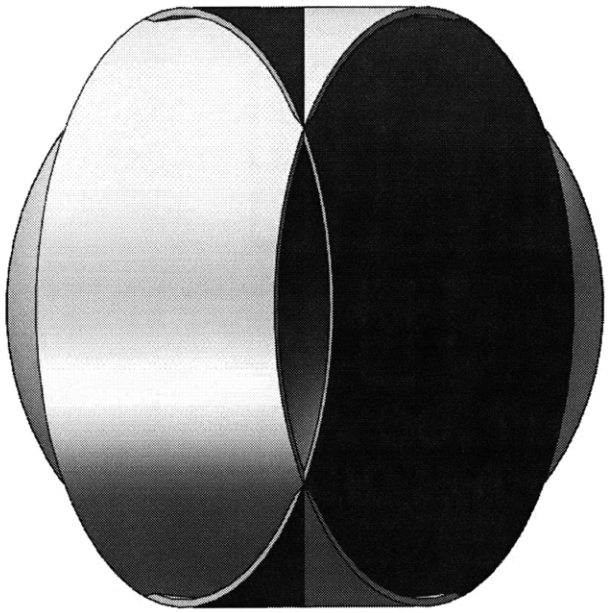

Figure 6-3: Connection Arm Access Envelope

As can be seen in Figure 6-3, the entrance to the tires inner space is widest at the

mid-height of the wheel, and gradually shrinks to a point upwards and downwards. This observation limits the size of the connection arm for the half-scale wheel-robot prototype. Schmitt avoided the design of a small connection arm by having the wheel-robot's steering axis offset from the wheel's center of gravity, allowing more room for the arm to connect to the steering actuator. Figure 6-4 provides a top view of the access envelope along with a measurement of the maximum width of the opening, shown to be only roughly 0.65 inches.

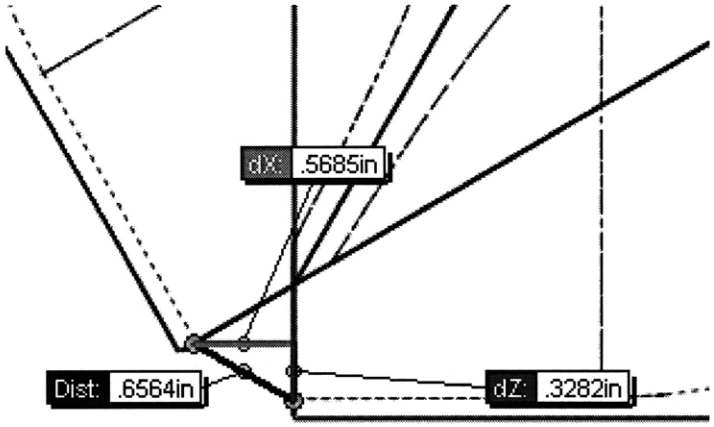

Figure 6-4: Maximum Envelope Width

6.3 Steering Actuator Placement

Originally, the steering motor was to be placed with its output shaft positioned vertically and aligned directly with the tires center of mass, allowing the wheel to steer about the center of the tires contact patch. Figure 6-10a illustrates the intended general placement of the steering motors output shaft within the tires interior space.

The widest part of the opening to the tires inside volume is barely over half an inch. This means that the connection arm, in order to not interfere with the steering range of the wheel, is limited to a maximum width of about half an inch, and its width must taper down along its height in order to fit in the access envelope illustrated in Figure 6-3. Therefore, in order to have the output shaft of the chosen AME steering

motor align with the center of gravity of the wheel and have the motor body rigidly attached to the connection arm, the motor must be able to fit in the access envelope in Figure 6-3. The chosen motors dimensions, shown in Figure 17, show that doing so was impossible. Therefore, alternative solutions were investigated in order to prevent the tire walls from colliding with the chosen AME steering motor while still forcing the wheel to pivot about the center of its ground contact patch.

6.3.1 Placement Concept 1

One possible solution involves mounting the steering motor closer to the base of the connection arm, nearer to the car frame. Both a pulley belt system [Figure 6-5a] and a gear train configuration [Figure 6-5b] were considered to transmit the steering motors torque to the wheel.

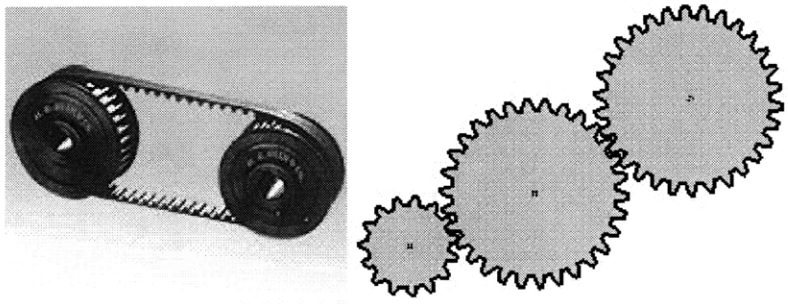

(a) Pulley Transmission [5] (b) Gear Transmission [19]

Figure 6-5: Steering Transmission

A problem with both of these configurations involves the major increase in the systems backlash. In particular, the gear train configuration increases backlash with every gear added in the line. Backlash in the steering results in less control over the angle the wheel-robots make relative to the car frame. This strips the driver of complete control over the handling of the CityCar and degrades the driving experience while putting the passengers at risk of an accident.

6.3.2 Placement Concept 2

Another possible solution involves using a custom-designed 4-bar linkage to connect the center of the wheel to the steering motor, located a short distance away from the wheels center. The concept of using a 4-bar linkage in the wheel-robot is illustrated in Figure 6-6a through Figure 6-6d, which show the linkage movement as the front left wheel-robot spans the entire steering range. The AME output shaft drives the input link, highlighted in dark green. The coupling between the drive motor and the connection linkage acts as the follower link, and mimics the rotation of the input link. As the coupling rotates, it pivots the wheel about the desired steering axis, which intersects with the wheel's center of gravity.

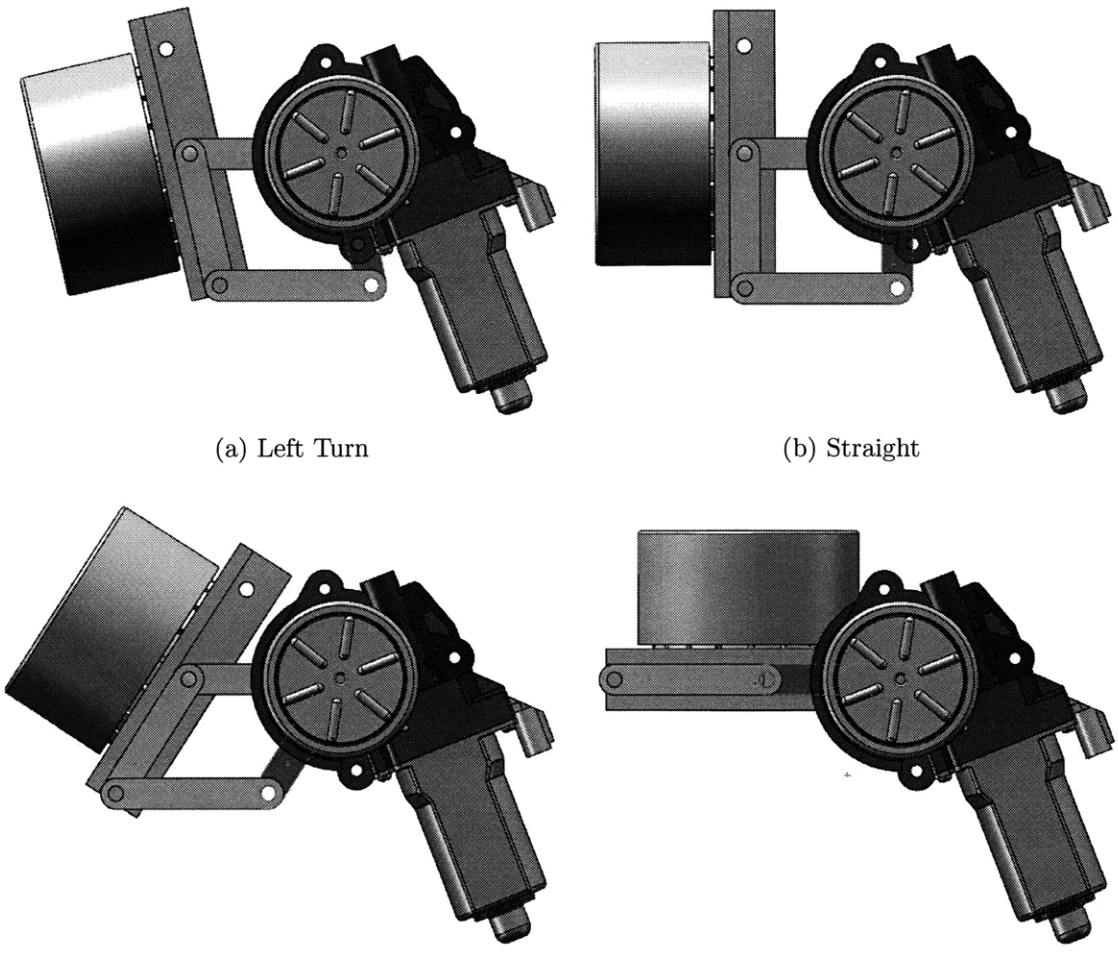

(a) Left Turn

(b) Straight

(c) Right Turn

(d) Sideways

Figure 6-6: Short 4-Bar Linkage Steering Range

Problems with this configuration arise due to the steering range of the wheel-robot. The first problem is the fact that the wheel-robot is supposed to be able to turn inward by 105 degrees. The 4-bar linkage design, however, limits the rotation of the input link to only 90 degrees, as seen in Figure 6-6d. While this is not a major problem, it does partially restrict the mobility of the CityCar when trying to parallel park.

The second problem is seen as the front left wheel progressively makes its clockwise turn illustrated in Figure 6-6c. The tires radial width, which is the total thickness of the tire with the spoke length included, collides with the steering motor as the tire steers inward. This interference, shown in Figure 6-7, disqualifies this concept from being considered for the half-scale prototype, as it does not even allow a 90 degree turn inward, let alone 105 degrees inward. The links are too short and therefore the steering motor is well within the work volume of the tire as it rotates about its center contact point with the ground. This discovery lead to the concept of using longer links, which is discussed in the next concept.

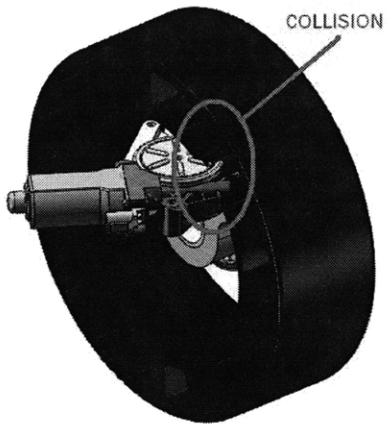

Figure 6-7: Short Linkage Collision With Tire

6.3.3 Placement Concept 3

A variant to Concept 2, this idea involved increasing the distance between the AME output shaft and the steering axis. In this iteration, the ground link and coupler link

were lengthened and bent as illustrated in Figure 6-8a through Figure 6-8d. Their modified forms provided the needed space for the tires radial width as the wheel turned 90 degrees inward.

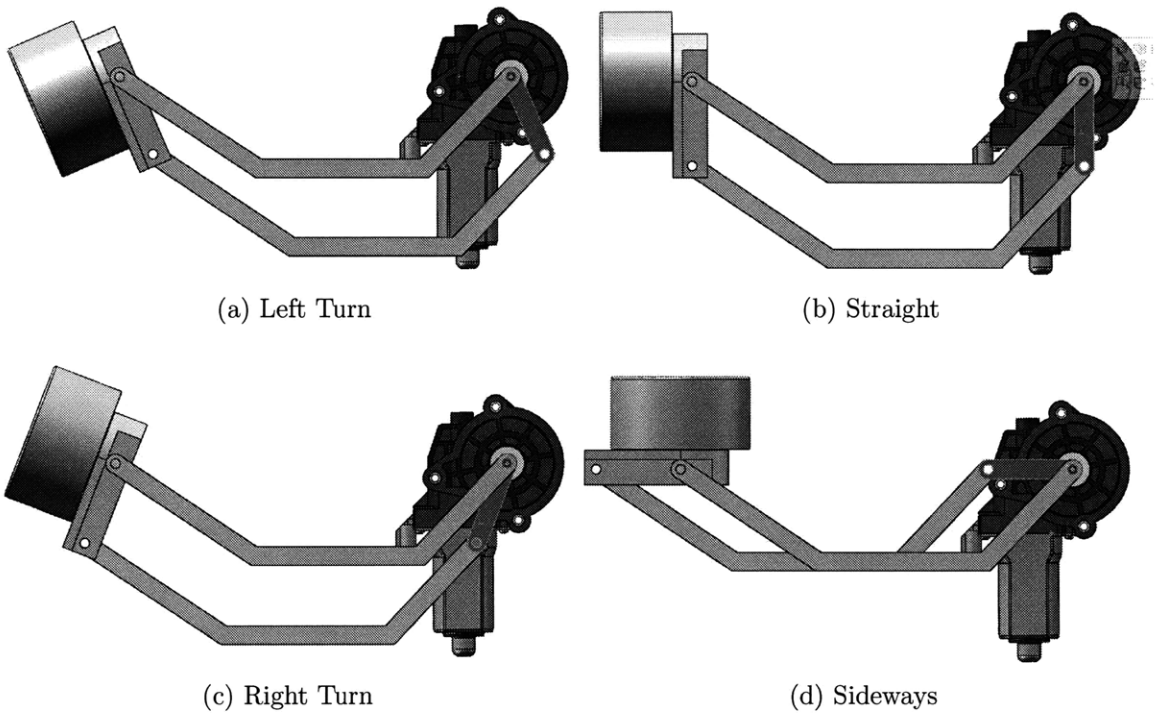

(a) Left Turn

(b) Straight

(c) Right Turn

(d) Sideways

Figure 6-8: Bent 4-Bar Linkage Steering Range

Problems with this configuration once again arise due to the steering range of the wheel-robot. The first problem is the fact that this 4-bar linkage design still limits the rotation of the input link to only 90 degrees, as seen in Figure 6-8d. While this is still not a major problem, it does partially restrict the mobility of the CityCar when trying to parallel park. Another problem with this configuration once again due to the steering range of the wheel-robot. As the front left wheel makes its counterclockwise turn illustrated in Figure 6-8a, the steering motor collides with the spokes located in the tires radial width. This interference, shown in Figure 6-9, disqualifies this concept from being considered for the half-scale prototype.

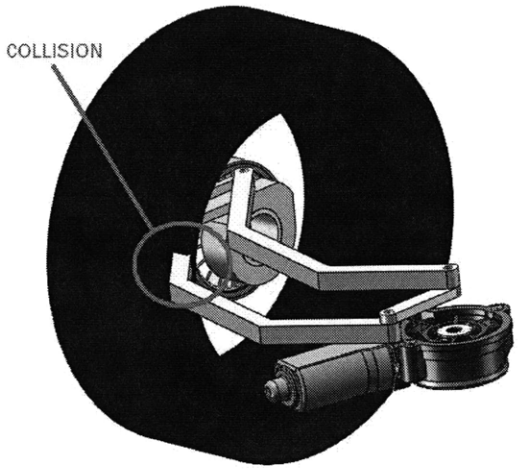

Figure 6-9: Bent Linkage Collision With Tire

6.3.4 Placement Concept 4

Another possible solution involves physically attaching the body of the steering motor to the drive motors fixed stator, and coupling the steering motors output shaft to the end of the connection arm. With this setup, the output shaft stays stationary relative to the connection arm reference frame while the AME motor body moves with the wheel as the wheel-robot is steered. The steering motor body will therefore never get in the way of the pivoting wheel as it steers, as Figure 6-10a and Figure 6-10b demonstrate.

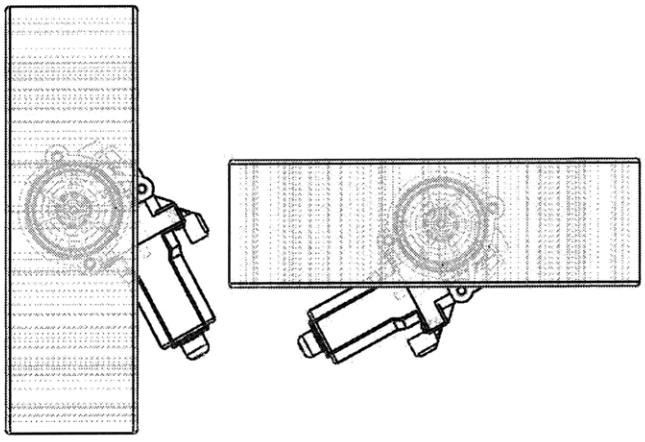

(a) Straight (b) Right-Angle

Figure 6-10: Steering Motor Following Tire

A challenge with this configuration is finding out how to have the connection arm couple with the output shaft while still having the steering motor body mount to the drive motors stationary stator. Due to the size of the AME steering motor, which takes up a considerable amount of the empty central volume of the wheel space, designing a connection arm end to grip onto the output shaft was a very difficult challenge. While Concept 4 is most likely the best way to avoid having the steering motor interfere with the rotating tire, more time needs to be spent on developing a proper coupling.

6.4 Drive Motor Hub

The large size of the chosen 36V drive motor consumed a large portion of the the available space inside the wheel-robot, as Figure 6-11a illustrates. Therefore, in order to provide space for the AME steering motor to fit, the drive motor was translated deeper in the wheel, until part of its rotating casing stuck out the back of the wheel, as Figure 6-11b illustrates. This method had been executed on earlier versions of full-scale wheel-robots and therefore the group was content with this design.

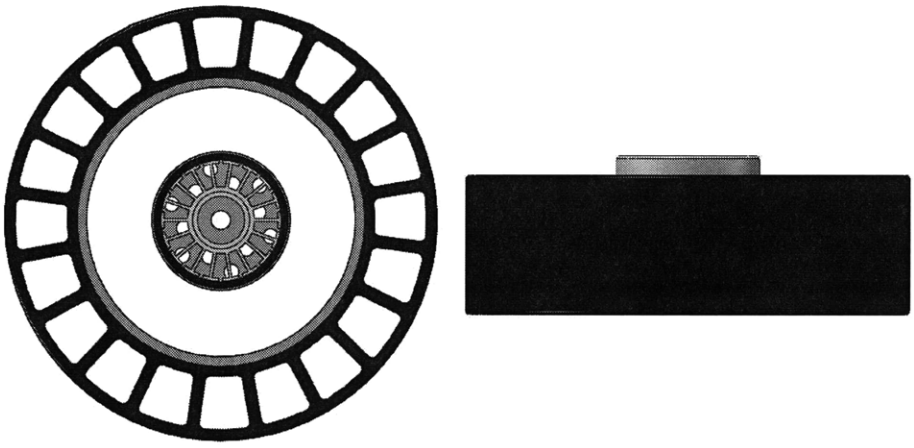

(a) (Front View) (b) (Top View)

Figure 6-11: Drive Motor Inside Wheel-Robot

The drive motor acted as the hub of the wheel robot, and metal spoke-like fins were

fabricated that connected the drive motor to the cylindrical rim fastened to the wheel's inner diameter. When the wheel-robot is static, the lower steel fins support the hub motor, which in turn support the higher fins, giving the tire its structure. The fins were cut on on a waterjet at the Media Lab and were fit onto the motor at a slight angle relative to the face of the hub. This design allows air to circulate inside the wheel-robot as it drives, propelling the fins through the air like a intake fan. The circulating air thus aides in keeping the drive motor cool while driving. Figure 6-12a shows the fins being assembled into the steel rim [Figure 6-12b] that connects the hub drive motor to the aluminum cylindrical frame that will adhere to the inside of the cast rubber tire. Figure 6-12c shows the inside of the wheel-robot and how the drive motor sits concentrically in the center of the newly fabricated steel hub rim.

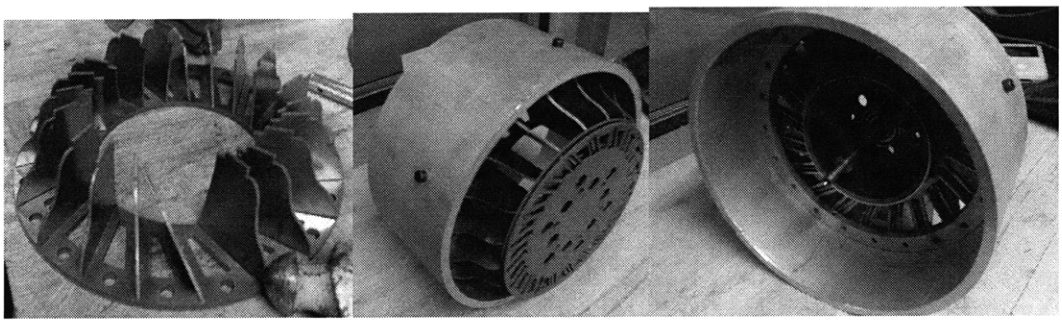

(a) Fin Assembly (b) Hub Rim (c) Drive Motor Support

Figure 6-12: Hub Motor Rim Fabrication

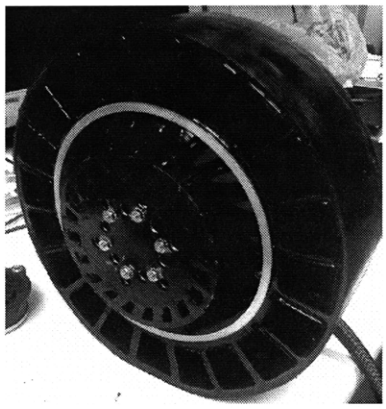

Figure 6-13: Fabricated Wheel-Robot Tire & Hub Rim

6.5 Conclusions

Wheel-robot integration is a difficult and multi-layered challenge, but it is also very interesting. Although the focus of this project was to find a stronger steering actuator and move the steering axis to be in-line with the tire's center of mass, exploration into the other aspects of the wheel-robot project could not be contained. As this report has demonstrated, much time has been spent in all areas of the wheel-robot design, but not nearly enough to finalize an overall design. Ideas and speculations on possible future design considerations have been addressed and new views on certain parameters of the project have been expressed. Although a final design for the placement of the steering motor was not resolved, much was learned about the design constraints that never came to mind in earlier iterations of the project. The design process has provided a much appreciated experience in the use of existing technologies toward innovational ideas and endeavors. The CityCar, along with the GreenWheel and the RoboScooter, is full of possibilities in how far the project can expand and mature throughout the upcoming years.

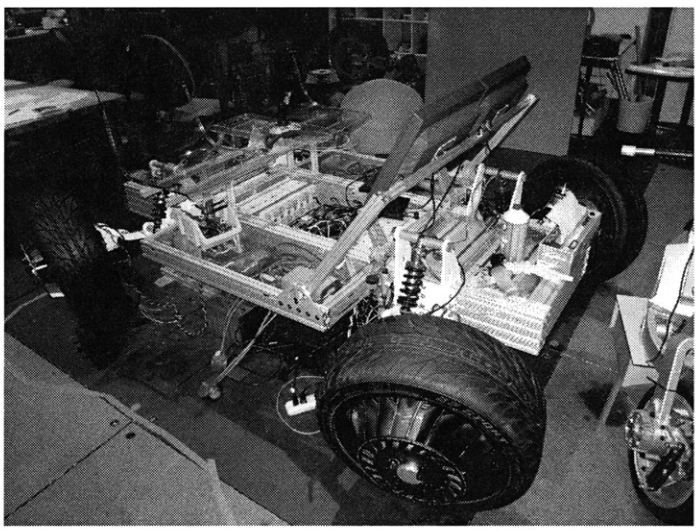

Figure 6-14: Full-Scale City Car Frame & Wheel-Robots

Bibliography

[1] A-Main Hobbies. Scanner RC Brushless Outrunner Motor. http://www.amainhobbies.com.

[2] A-Main Objectives. HSR-5995TG Digital Robotic Servo with Titanium Gears. http://www.amainobj.com/index.php?act=viewProd&productId=50, 2006.

[3] Alexander H. Slocum, Sr. Design Handbook: Motor Torque Speed & Power, Wheels, and Winches. http://pergatory.mit.edu/2.007archive/Resources/calculations/motorcalc/motorcalc.html, 2009.

[4] AM Equipment. 210 Series Motor. http://amequipment.com/PDFFiles/801-1007.pdf, 2003.

[5] H. G. Shah & Co. Automobile Components. http://www.indiamart.com/hg-shah/automobile-components.html.

[6] Paul Haney. The Racing & High-Performance Tire. *Sports Car Magazine*, 2004.

[7] Michael Chia-Liang Lin. GreenWheel & RoboScooter.

[8] William J. Mitchell. http://cities.media.mit.edu/.

[9] Karen Nice. How Gears Work. http://science.howstuffworks.com/gear.htm, 2000.

[10] OnDrives Precision Manufacturing. Wormwheel Gearbox: P20 Type. http://www.ondrives.com/products.asp?recnumber=214, 2009.

[11] Timothy B. Rhyne and Steven M. Cron. Development of a Non-Pneumatic Wheel. *Tire Science & Technology*, 34:150–169, September 2006.

[12] Georg Rill and Cornelius Chucholowski. A Modeling Technique for Fast Computer Simulations of Configurable Vehicle Systems. http://fluid.ippt.gov.pl/ictam04/text/sessions/docs/SM26/11672/SM26_11672.pdf.

[13] Peter Schmitt. Just Build It! A Fully Functional Concept Vehicle Using Robotic Wheels. Master's thesis, M.I.T., June 2007.

[14] Smart®. http://www.smartusa.com/.

[15] Curt Thurston. http://www.curtthurston.com/3DHTML/LinearDrive.html.

[16] Tsikot. Honda Offers Suspension Makeover Treats. http://www.tsikot.com/honda-offers-suspension-makeover-treats/.

[17] Vespa Speed. Rear Shock, TP, ET4. http://vespaspeed.com/shop/index.php?main_page=product_info&cPath=1_2_25&products_id=51&zenid=nrmkae5cpmb4iptv7p222mn9q6, 2005.

[18] William Lark, Jr. CityCar.

[19] Zhang, Yi. Introduction to Mechanisms. http://www.cs.cmu.edu/~rapidproto/mechanisms/examples.html.